

for roughly 7 percent of the total aerosol mass in the cloud layer on 5 May 1982. The depolarization ratios calculated by Hayashida and coworkers start to drop from the maximum of 20 percent before about mid-May 1982, which is roughly in agreement with the time expected for the NaCl particles to start converting and disappearing from the atmosphere.

It is not clear how widespread the occurrence of halite may be in eruption clouds, but our data suggest that it may be specifically favored in alkalic volcanoes. The mildly alkalic El Chichón magma contains higher amounts of chloride (as well as sulfur) compared to other eruptions (Table 2), so that it is reasonable to expect a more prominent role for chloride components. The El Chichón magma volatilizes gaseous NaCl and probably other elements (9), and in the eruption cloud the NaCl forms halite aerosols (10). NaCl is also a common fumarolic incrustation at volcanoes (11). Analysis of materials absorbed on the ash of El Chichón (12) indicates an average of 355 parts per million (ppm) of sodium and 780 ppm of chloride, which is consistent with the presence of halite in the eruption cloud. The earlier idea that the unusual volatile signature of El Chichón's magma was caused by interaction with underlying evaporites (13) has been apparently ruled out by isotopic studies (14), and the high content of chloride and sulfur of the magma is

thought to have a deeper origin. We have also found halite particles in volcanic plumes from Mount Erebus, Antarctica (15). Thus, although it has not been widely reported, halite probably forms in many eruption clouds but is most noticeable in the eruption of alkalic magmas.

#### References and Notes

1. R. L. Chuan, in *Fine Particles, Aerosol Generation, Measurement, Sampling, and Analysis*, B. Y. H. Liu, Ed. (Academic Press, New York, 1975), p. 763.
2. D. C. Woods and R. L. Chuan, *Geophys. Res. Lett.* **10**, 1041 (1983).
3. R. L. Chuan and D. C. Woods, *Geophys. Res. Lett.* **10**, 335 (1983).
4. G. K. Yue, V. A. Hohnen, C. S. Kiang, *Water Air Soil Pollut.* **6**, 277 (1976).
5. S. Hayashida et al., *Water Research Institute, Middle Atmospheric Program*, note 3 (1984).
6. D. J. Hofmann and J. M. Rosen, *Geophys. Res. Lett.* **10**, 313 (1983).
7. W. G. Mankin and M. T. Coffey, *Science* **226**, 170 (1984).
8. B. W. Gandrud, private communications.
9. K. B. Krauskopf, *Econ. Geol.* **59**, 22 (1964).
10. J. N. Oskarsson, *J. Volcanol. Geotherm. Res.* **8**, 251 (1980).
11. R. E. Stoiber and W. I. Rose, *Geochim. Cosmochim. Acta* **38**, 495 (1974).
12. J. C. Varekamp, J. Luhr, K. Prestegard, *J. Volcanol. Geotherm. Res.* **23**, 39 (1984).
13. W. A. Duffield, R. A. Tilling, R. Canul, *ibid.* **20**, 117 (1984).
14. R. O. Rye, J. Luhr, M. O. Wassenwann, *Geol. Soc. Am. Abstr. Prog.* **16**, 642 (1984).
15. R. L. Chuan and W. I. Rose, unpublished results.
16. W. I. Rose, R. E. Stoiber, L. L. Malinconico, in *Andesites: Orogenic Andesite and Related Rocks*, R. S. Thorpe, Ed. (Wiley, New York, 1982), p. 669.
17. W. G. Melson, C. A. Hopson, C. F. Kienle, *Geol. Soc. Am. Abstr. Prog.* **12**, 461 (1980).
18. W. I. Rose et al., *J. Volcanol. Geotherm. Res.* **17**, 133 (1983).
19. J. F. Lure, I. S. E. Carmichael, J. G. Varekamp, *ibid.* **23**, 69 (1984).

14 March 1985; accepted 26 July 1985

## Oroclinal Bending of the Southern Sierra Nevada Batholith

**Abstract.** *Structural, magmatic, and isotopic features of the southern Sierra Nevada batholith are deflected clockwise with respect to its central and northern parts. Directions of magnetization at three localities in the southern Sierra Nevada are progressively deflected; this is consistent with the hypothesis that the region was tectonically rotated in an orocline. No paleomagnetic deflection was observed northwest of the White Wolf-Kern Canyon fault system. Oroclinal bending of a block bounded by the San Andreas, Garlock, and White Wolf-Kern Canyon faults may have occurred before about  $16 \times 10^6$  years ago. The deformation may have been a response to shear at the western boundary of the North American plate caused by oblique subduction.*

MICHAEL McWILLIAMS

YIANPING LI

Department of Geophysics,  
Stanford University,  
Stanford, California 94305

Structural, magmatic, and isotopic patterns of the northern and central Sierra Nevada batholith of California have nominal northwest-southeast trends, but to the south these features are systematically deflected clockwise (1-4). The deflection approaches 90° at the southernmost end of the batholith, where struc-

tures of the Tehachapi and San Emigdio Mountains have an east-west trend (Fig. 1). This observation has led to suggestions that the magmatic and isotopic patterns in the south were once approximately parallel to those of the northern and central Sierra Nevada but were subsequently deflected during post-Cretaceous tectonic activity (4-6).

Paleomagnetic data (7) suggest that part of the Bear Valley Springs pluton (age,  $80 \times 10^6$  to  $86 \times 10^6$  years) (locality 3 in Fig. 1) has rotated clockwise  $45^\circ \pm 14^\circ$ ; this is consistent with the in-

ferred tectonic flexure. Miocene strata that overlie the pluton show no rotation, constraining the time of deformation to later than  $80 \times 10^6$  years ago but earlier than  $16 \times 10^6$  years ago (8).

One key question is whether the observed deflection of paleomagnetic vectors was caused by oroclinal bending or by another process. The aberrant magnetizations could reflect movement of an independent block that was tilted or rotated, rather than flexure of the entire southern Sierra Nevada Batholith (9).

To discover whether oroclinal bending was the cause, we made paleomagnetic measurements at three points in the southern Sierra Nevada (localities 1, 2, and 4 in Fig. 1). If the orocline hypothesis is correct, a systematic increase in paleomagnetic deflection with distance should be observed along the trend of the southern Sierra Nevada. If the observed 45° deflection resulted from movement of an isolated block, a systematic trend in the deflection of paleomagnetic directions would be absent.

At locality 1 (Fig. 1) we collected biotite granodiorite samples from the Claraville pluton. At locality 2 we collected samples of hornblende-biotite tonalite from the Bear Valley Springs pluton. Both plutons are of late Cretaceous age. Biotite K:Ar ages for the Bear Valley Springs pluton range from  $81 \times 10^6$  to  $86 \times 10^6$  years, and biotite K:Ar ages from the Claraville pluton are  $75 \times 10^6$  and  $79 \times 10^6$  years (4). Localities 2 and 3 sample the same pluton but lie on opposite sides of the White Wolf-Kern Canyon (WWKC) fault.

At localities 1 and 2, no clear ancient horizontal reference is available because there are no younger strata in contact with basement rocks nearby from which to obtain estimates of the total amount of post-Cretaceous tectonic tilt. At locality 3, estimates of post-Miocene tectonic tilt were obtained from attitudes of nearby Miocene strata (7). At locality 4, the basement rocks are overlaid by Paleocene to Miocene strata, which provide an  $(18 \pm 2) \times 10^6$  year (10) horizontal reference. Here, we sampled garnet-bearing tonalite, amphibolite, and gneiss, for which biotite K:Ar ages range from  $77 \times 10^6$  to  $87 \times 10^6$  years.

At each locality, samples were collected at a number of sites representing an outcrop area of about 10 m<sup>2</sup>. Five individually oriented cores were drilled at nearly every site and oriented with solar compass and clinometer (accuracy,  $\pm 2^\circ$ ). One specimen cut from each sample was subjected to stepwise alternating field (AF) demagnetization in peak fields up to 75 mT. Representative specimens

Table 1. Late Cretaceous magnetization directions.  $\kappa$  is the precision parameter,  $\alpha_{95}$  is the radius of the 95 percent confidence circle, and  $R \pm \Delta R$  is the apparent rotation and 95 percent confidence limit (18). Corrections have been made for the estimated post-Miocene tilt at localities 3 and 4.

Locality	Age (years $\times 10^6$ )	Sites (number)	Samples (number)	Declination (degrees)	Inclination (degrees)	$\kappa$	$\alpha_{95}$ (degrees)	$R \pm \Delta R$ (degrees)
1	79 to 75	4	19	355.9	57.8	46	14	$20 \pm 24$
2	86 to 81	16	69	336.5	68.1	169	3	$0 \pm 13$
3	86 to 81	8	34	22.3	55.7	97	6	$45 \pm 14$
4	87 to 77	10	50	34.5	56.0	38	8	$59 \pm 16$

from each site were subjected to stepwise thermal demagnetization at temperatures up to 620°C.

Stable, well-grouped directions of magnetizations were isolated in most samples after removal of a low-coercive force magnetization parallel to the present geomagnetic field direction, which was probably a viscous remanence mag-

netization (Fig. 2). Results from 9 percent of the collection were discarded because a stable magnetization could not be resolved during the demagnetization experiments.

The mean magnetization directions measured at each locality are summarized in Table 1 and plotted in Fig. 3. Each mean direction represents a vector

average of the individual site mean directions. A site mean direction represents an "instantaneous" recording of the ancient geomagnetic field. Averaging individual directions within each site minimizes the effects of core orientation error. If the natural remanent magnetization is of thermoremanent origin, then the site mean direction dates the time

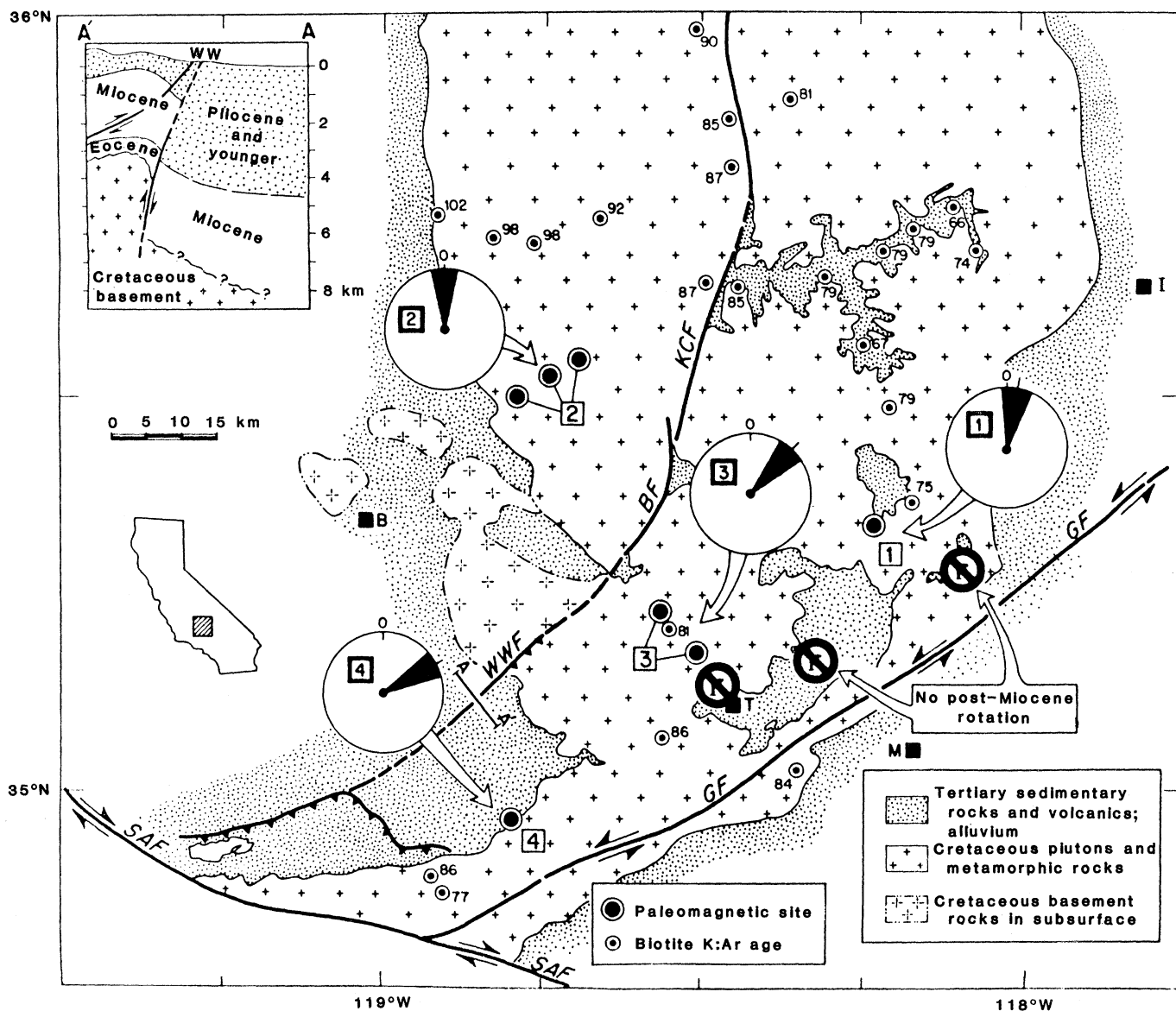


Fig. 1. Schematic geological map of the southern Sierra Nevada [from (4)]. Apparent rotation is denoted by filled wedge in circular plot. Center of wedge points directly north when  $R$  (rotation) is  $0^\circ$  (that is, when there is no apparent rotation). Angle subtended by wedge denotes uncertainty in  $R$  at the 95 percent confidence level. Faults: BF, Breckenridge; GF, Garlock; KCF, Kern Canyon; SAF, San Andreas; WWF, White Wolf. Geographic references: B, Bakersfield; I, Inyokern; M, Mojave.

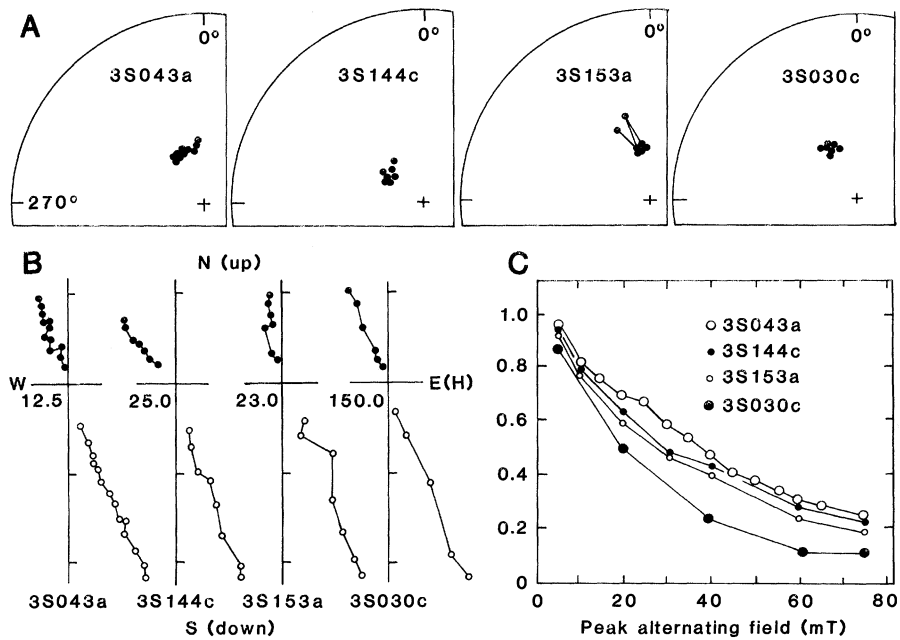


Fig. 2. Examples of AF demagnetization for four specimens from locality 2. (A) Stereographic projection of magnetization directions during progressive treatment to 75 mT. (B) Orthogonal projection of vector end points for the same samples. Solid symbols denote projection on the horizontal plane; open symbols denote vertical versus horizontal component. Scale for axis ticks at lower left of origin is in  $10^{-3}$  A/m. (C) Normalized intensity plotted against peak demagnetizing field.

when the rock cooled below a critical blocking temperature. By averaging site mean magnetization directions, bias due to geomagnetic secular variation should be minimized.

The paleomagnetic results are consistent with the hypothesis that the southern Sierra Nevada has undergone oroclinal bending. At locality 1, where little or no deflection is predicted, the measured magnetizations were virtually indistinguishable from values for the central Sierra Nevada (11). At localities 3 and 4, progressively increasing deflections of  $45^\circ \pm 14^\circ$  and  $59^\circ \pm 16^\circ$  were observed, which are well in excess of the estimated experimental errors.

In contrast, the paleomagnetic directions from locality 3 (northwest of WWKC) showed no apparent clockwise deflection. A plausible explanation is that WWKC delineates the northern and western limits of the orocline. This is consistent with the observation that WWKC is in places a high-angle reverse fault (12, 13) that may have thrust the Tehachapi-San Emigdio domain over unrotated basement terranes to the north and west. If WWKC becomes shallower with increasing depth, then it and the San Andreas, Garlock, and Sierra Nevada faults may delineate the present boundaries of the orocline. Displacement may have occurred along a horizontal to subhorizontal detachment zone at a depth of 5 to 10 km (inset in Fig. 1). If this interpretation is correct, then

source and reservoir rocks in the San Joaquin valley have been thrust beneath older granitic basement.

The timing of the deflection is not tightly constrained. Data from Miocene volcanic and sedimentary rocks near locality 3 suggest no major tectonic rotation more recent than  $16 \times 10^6$  years ago, and thus the age of deformation in the easternmost part of the rotated domain is constrained to be older than  $16 \times 10^6$  years but younger than  $80 \times 10^6$  years. Thrust movement along the White Wolf fault system may account for the observed deflection, yet most

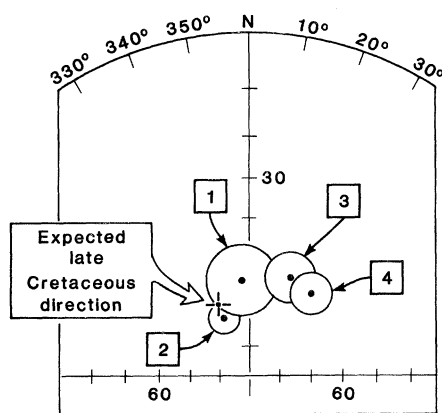


Fig. 3. Averaged magnetization directions from localities 1 to 4 (filled dots) compared with the expected late Cretaceous direction (cross). Circles denote 95 percent confidence limits. If no tectonic rotation had occurred, directions 3 and 4 would be indistinguishable from the expected direction.

White Wolf fault displacement has occurred since Miocene times (12).

Two potential solutions are apparent. If the observed paleomagnetic deflections result from post-Miocene rotation, then the White Wolf fault probably played a key role in the displacement, and a boundary must exist between the deflected Cretaceous sites at locality 3 and the undeflected Miocene sites immediately to the east (Fig. 1). No plausible boundaries are currently known, and potential candidates in the Tehachapi area display only very small displacements. Alternatively, if the observed paleomagnetic deflections occurred before about  $16 \times 10^6$  years ago, then Neogene White Wolf fault displacement was probably not critically linked to the tectonic rotation; however, pre-Neogene motion may be responsible in part. Displacement on the Kern Canyon fault, which was active in Cretaceous times but has been inactive for about  $3.5 \times 10^6$  years (14), may also be linked to the observed paleomagnetic deflection. If the deflection is indeed pre-Miocene in age, Cretaceous basement rocks may occur below the surface trace of the White Wolf fault in the footwall block. These are present in reconstructions made from borehole data (12, 13), suggesting that rotation occurred before major movement on the White Wolf fault. The proposal of pre-Miocene rotation may be supported if rotated Cretaceous basement rocks are found to the south of the Garlock fault, upon which motion began about  $17 \times 10^6$  years ago (4).

The driving mechanism may involve shear distributed at the plate boundary (15) by North American-Kula, North American-Farallon, or North American-Pacific plate interaction (or all three). If flexure occurred prior to passage of the Mendocino triple junction ( $\sim 23 \times 10^6$  years ago), deformation of the southern Sierra Nevada could be linked to a right-lateral component of motion produced by oblique subduction of the Kula or Farallon plates (16), or it might be related to proto-San Andreas motion (17). A shallowly dipping Kula slab seems to be a better candidate for the driving force because the tangential component of North American-Farallon plate motion is relatively small in the southern Sierra Nevada between  $30 \times 10^6$  and  $70 \times 10^6$  years. After  $23 \times 10^6$  years, North American-Pacific plate motion and the early San Andreas transform fault may have developed sufficiently to generate the necessary right-lateral motion, but the relatively weak plate coupling (16) and narrow time window ( $\sim 5 \times 10^6$  years) make this a less likely explanation.

tion. Alternatively, as the Mendocino triple junction passed, a "tectonic snow plow" created by the differential topography of juxtaposed old and young oceanic lithosphere at a transform fault may be a credible driving mechanism, depending on the depth to which such a feature might persist.

#### References and Notes

1. J. G. Moore, *J. Geol.* **67**, 197 (1959).
2. J. F. Evernden and R. W. Kistler, *U.S. Geol. Surv. Prof. Pap.* **623** (1970).
3. R. W. Kistler and Z. E. Peterman, *U.S. Geol. Surv. Prof. Pap.* **1071** (1973).
4. D. C. Ross, *U.S. Geol. Surv. Open File Rep.* **80-307** (1980).
5. A. Locke, *Geol. Soc. Am. Bull.* **51**, 513 (1940).
6. B. C. Burchfiel and G. A. Davis, in *The Geotectonic Development of California*, W. G. Ernst, Ed. (Prentice-Hall, Englewood Cliffs, N.J., 1981), pp. 217-252.
7. L. R. Kanter and M. McWilliams, *J. Geophys. Res.* **87**, 3819 (1982).

8. B. Turrin, unpublished data.
9. M. McWilliams, *Rev. Geophys. Space Phys.* **21**, 644 (1983).
10. J. G. Vedder, D. G. Howell, J. A. Forman, *Soc. Econ. Paleontol. Mineral. Pacific Sect. Paleogeogr. Symp.* **3**, 239 (1979).
11. L. S. Frei, J. R. Magill, A. Cox, *Tectonics* **3**, 157 (1984).
12. R. S. Stein and W. Thatcher, *J. Geophys. Res.* **86**, 4913 (1981).
13. T. M. Harrison and K. Bé, *Earth Planet. Sci. Lett.* **64**, 244 (1983).
14. J. L. Burnett, *California Division of Mines and Geology Map Sheet 35* (1976).
15. M. E. Beck, *Tectonophysics* **93**, 1 (1983).
16. B. M. Page and D. C. Engebretson, *Tectonics* **3**, 133 (1984).
17. T. H. Nilsen, *Soc. Econ. Paleontol. Mineral. Pacific Sect. Field Trip Guideb.* **2**, 7 (1973).
18. M. McWilliams, *Geophys. Res. Lett.* **11**, 825 (1984).
19. We thank M. Fones, P. Layer, and J. Tarduno for help with sample collection; D. Ross for advice on site selection and preprints of geological maps; and M. Basher of the California Department of Water Resources for permission to collect samples. Supported by NSF and the Petroleum Research Fund.

20 September 1984; accepted 12 July 1985

## Dust Devils on Mars

**Abstract.** Columnar, cone-shaped, and funnel-shaped clouds rising 1 to 6 kilometers above the surface of Mars have been identified in Viking Orbiter images. They are interpreted as dust devils, confirming predictions of their occurrence on Mars and giving evidence of a specific form of dust entrainment.

PETER THOMAS

PETER J. GIERASCH

Center for Radiophysics and  
Space Research, Cornell University,  
Ithaca, New York 14853

One of the major geologic processes on Mars is the entrainment and transportation of dust by winds, but spacecraft

observations of the genesis and development of local and global dust storms on Mars are sparse (1), and the specific conditions necessary for dust entrainment are poorly known (2). It has long been suspected that dust devils occur on Mars and that they may be important in the initiation of large dust storms or in increasing the general atmospheric dust

content (3). We now report the discovery of dust devils in Viking Orbiter images; this finding provides an important documentation of a specific form of dust entrainment by winds on Mars.

Dust devils have meteorological as well as geological significance. Fluid motions in an atmospheric boundary layer can be driven either by stresses due to the mean wind (forced convection) or by buoyancy due to heating of the gas adjacent to the surface (free convection) (4). Dust devils are an example of the latter. On Earth, large-scale eolian transport is generally due to forced convection. Moderate to high winds characterize forced convection, and on Mars, where the atmospheric density is only about 1 percent of that on Earth, it is estimated that winds must exceed about 25 to 40 m sec<sup>-1</sup> to initiate soil movement (5). Because near-surface winds this strong are rare (6), it is of great interest to discover that other modes of dust entrainment are acting.

Small bright clouds with long, tapered shadows (Fig. 1), distinctive forms among the many albedo and atmospheric features observed on Mars, were initially found during mapping of linear wind streaks in Amazonis Planitia. A search was then made of all Viking Orbiter images for other dust devils. Criteria for positive identification of a feature as a dust devil were (i) an elongated shape, (ii) a nearly vertical orientation, and (iii) transience. The first two criteria rule out cumulus clouds or streaks of windblown

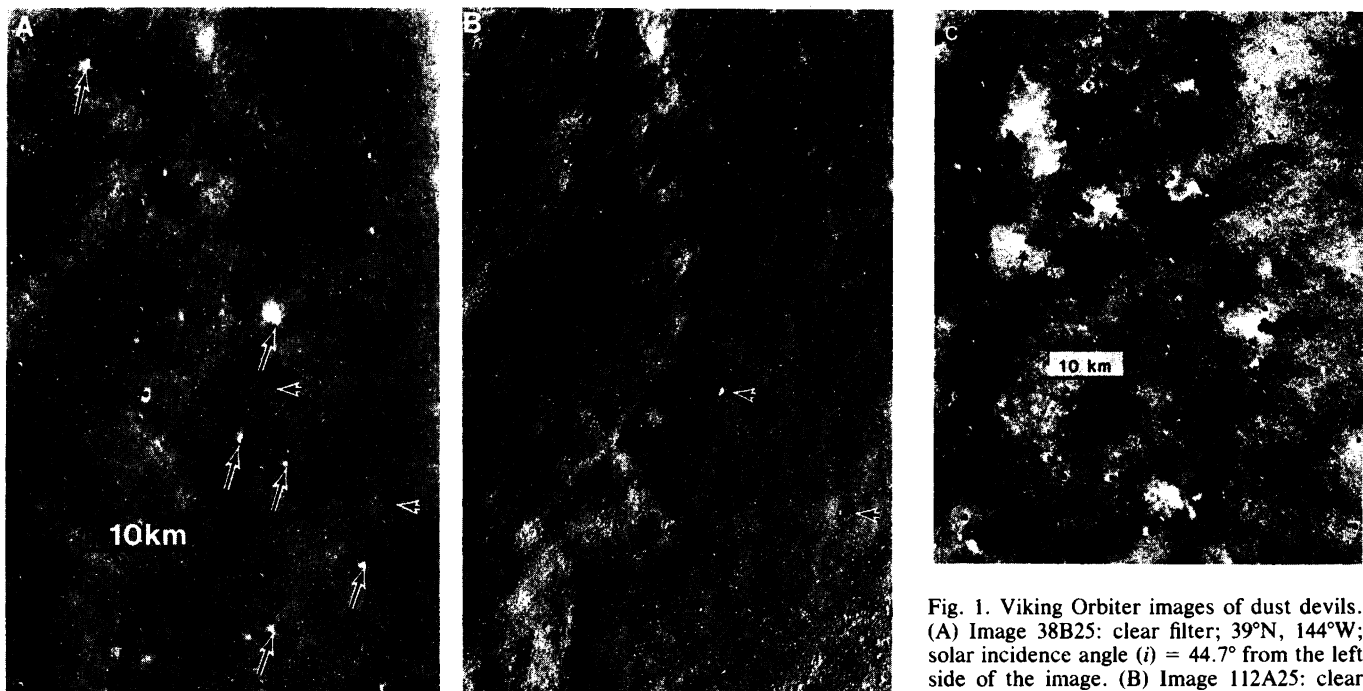


Fig. 1. Viking Orbiter images of dust devils. (A) Image 38B25: clear filter; 39°N, 144°W; solar incidence angle ( $i$ ) = 44.7° from the left side of the image. (B) Image 112A25: clear filter; same area as (A);  $i$  = 76.4°. Comparison shows which features are variable and which are topographic forms. Dust devils are shown by large arrows; small arrowheads show two craters visible in (B). (C) Image 34B01: clear filter; 36°N, 153°W;  $i$  = 38.6°. Dust devils are identified by arrows.

son shows which features are variable and which are topographic forms. Dust devils are shown by large arrows; small arrowheads show two craters visible in (B).